

Multi-Stage Formation of Apatite in the Early Proterozoic Metagabbroids of the Velimyaki Massif (the Northern Ladoga Region)

R. L. Anisimov^{a, *}, Sh. K. Baltybaev^{a, b}, I. M. Vasilyeva^a,
N. G. Rizvanova^a, O. L. Galankina^a, and V. M. Savatenkov^{a, b}

^a *Institute of Precambrian Geology and Geochronology, Russian Academy of Sciences, St Petersburg, 199034 Russia*

^b *St. Petersburg State University, Institute of Earth Sciences, St. Petersburg, 199034 Russia*

*e-mail: romjulleoanis@mail.ru

Received August 22, 2025; revised September 28, 2025; accepted October 10, 2025

Abstract—The Early Proterozoic Velimyaki gabbroid massif of the Northern Ladoga region was formed in two intrusive phases. The rocks of the first and second intrusive phases contain apatite, which forms ore clusters together with magnetite and ilmenite in pyroxenites and monzogabbros of the first phase or in monzodiorites and monzonites of the second phase. Modeling of magmatic mineral formation suggests that the rocks of phases I and II originated from a single parent melt through fractional crystallization. The results of metamorphic modeling are consistent with the presence of two stages of metamorphic alteration of the rocks: an earlier low-temperature stage (replacement of clinopyroxene by actinolite) and a later medium-temperature stage (formation of green hornblende rims). Further study of apatite in the rocks of the second phase (monzodiorites and monzonites) shows that the U–Pb apatite system demonstrates stages of postmagmatic mineral formation during 1.80–1.81 Ga regional metamorphism. The ages and genesis of the apatite are consistent with its morphology and paragenetic relationships with titanite, actinolite, green hornblende, acid plagioclase and quartz, which formed during regional metamorphism. Sm–Nd isotope analysis of hornblende and titanite from the host amphibolites also indicates the manifestation of regional metamorphism about 1.84–1.80 Ga ago.

Keywords: apatite, gabbroids, metamorphism, Northern Ladoga area, Pb–Pb system, dating

DOI: 10.1134/S0016702925601020

INTRODUCTION

Apatite $\text{Ca}_5(\text{PO}_4)_3(\text{F}, \text{Cl}, \text{OH})$ in the mafic magmatic rocks (basalts, gabbros, and others) crystallizes at different stages of mineral formation depending on the definite geological settings and a change of thermodynamic conditions (Piccoli and Candela, 2002; Webster and Piccoli, 2015; Harlov, 2015, and others). For this reason, apatite serves not only as indicator of geochemical environment of mineral formation, but also as geochronometer recording the stages of crystallization or recrystallization of host rock (Kirkland et al., 2018). U–Pb apatite system applied for dating of mafic magmatic rocks (Marfin et al., 2021) is constrained by its chemical stability, uranium and lead contents, and influence of postmagmatic processes.

Apatite could crystallize one of the first accessory minerals at the early stages of magma differentiation, together with chromite, magnetite, and olivine. In mafic melts, it forms at relatively high temperatures (1000–1100°C, Kieffer et al., 2024).

The solubility of apatite in a melt increases with decreasing silica (Watson, 1979). The different degree

of apatite solubility is likely expressed in varying amounts of this mineral in differentiated magmatic rocks. In the layered intrusions, for instance, in gabbronorite complexes, cumulus apatite enriches the upper portions of the intrusions, forming apatite–magnetite ores (Kärkkäinen and Appelqvist, 1999; Kieffer et al., 2024), whereas intercumulus apatite sometimes occurs in the lower zones together with Fe–Ti–V, Cu–Ni–PGE, and Cr mineralization (Boudreau et al., 1986; Kieffer et al., 2024).

In gabbroid rocks, apatite usually crystallizes with magmatic plagioclase and clinopyroxene, the crystallization temperature of which is no less than 800–1000°C (Boudreau et al., 1986; Kieffer et al., 2024). In such cases, it occurs as small inclusions in major silicates or in interstices. However, apatite is frequently formed at the late magmatic stage grading into hydrothermal–metasomatic stage, when residual fluids are enriched in (F, Cl, P, and others), thus facilitating the formation of large apatite grains, sometimes in vein form (Boudreau et al., 1986; Harlov, 2015). Apatite plays a special role in the carbonatite complexes related to the alkaline–ultrabasic magmas, in which it

could be major ore mineral, as it occurs, for instance, in the Khibinskiy massif (Kogarko, 2018).

Thus, apatite in magmatic rocks is formed at the magmatic crystallization stage, but its accumulations could be also related to the late- and post-magmatic and hydrothermal–metasomatic processes.

The object of this study is the Velimyaki clinopyroxenite–monzodiorite–monzonite massif in the Northern Ladoga region. Based on obtained ages (1891 ± 4.9 Ma, Bogachev et al., 1999) or 1894 ± 6 Ma (Alekseev and Kotova, 2010), the massif was formed at the early stage of the Svecofennian accretionary orogeny. Unlike other intrusive rocks of the Northern Ladoga region of the same age, this massif defines a subalkaline evolution trend, which is expressed in the elevated content of biotite and, in some rocks, K-feldspar. In addition, this massif is enriched in phosphorus accumulated in apatite, content of which reaches 4 wt % (Alekseev, 2008). Since 19th century, the massif has attracted attention by its titanomagnetite mineralization. Later, gold was discovered in metasomatites confined to the clinopyroxenite bodies (Alekseev, 2008). Understanding the reasons for differences of the Velimyaki massif from other subsimultaneous mafic intrusions, including also elevated apatite contents, could provide the deeper insight into the geological history of this region.

In the metamorphosed gabbroids of the Velimyaki massif, apatite has been studied previously in the rocks of the first intrusive phase (Baltybaev et al., 2024). The U–Pb dating revealed that the apatite recrystallized at 1790 ± 5 Ma, which is much younger than the age of 1894 ± 6 Ma dated by U–Pb zircon method (Alekseev, 2008; Alekseev and Kotova, 2010). The younger apatite age is related to the influence of regional metamorphism on the rocks of the Velimyaki massif. Such assumption was confirmed by the spatial association of apatite with hornblende–biotite accumulations, which were related to the metamorphic processes that spanned this massif. The recrystallization of apatite led to the formation of allanite grains near apatite through its exsolution (e.g., Harlov, 2015).

Later detailed petrographic and mineralogical studies showed that the elevated concentrations of apatite in the Velimyaki massif occur not only in the rocks of the first phase, but also in relatively acid varieties, monzodiorites and monzonites of the second phase. In addition, these more evolved rocks could contain apatites of different crystallization stages, likely magmatic and metamorphic. With allowance for these data, the comparative mineralogical and isotope–geochemical studies were carried out for morphologically different apatite grains from the second intrusive phase. Results of these studies are reported below.

In addition to U–Pb dating of apatites from rocks of the second phase, Sm–Nd isotope study was conducted for amphiboles and titanite from framework amphibolites that were metamorphosed together with the massif rocks in the Paleopaleoproterozoic.

METHODS

X-ray spectral fluorescence analysis of rocks was carried out on an ARL 9800 spectrometer (Switzerland) at the Laboratory of the Karpinsky Institute (St. Petersburg). Samples as pellets were obtained by sample mixing in 1 : 9 proportions with lithium metaborate and tetraborate (in equal fractions) and fusion in gold–platinum crucibles. The determinable oxide concentrations vary from 0.01 to 0.05 wt % depending on the measured component.

The mineral composition was analyzed on a JEOL JSM-6510LA scanning electron microscope equipped with EDS JEOL JED-2200 at the Institute of Precambrian Geology and Geochronology (IPGG) of the Russian Academy of Sciences (St. Petersburg). Standard samples represented by simple compounds and pure metals were used. Analyses were performed at 20 kV acceleration voltage and 1 nA beam current. The raw data were corrected using a ZAF matrix correction routine.

U–Pb isotope analysis of minerals was carried out at the Institute of Precambrian Geology and Geochronology (IPGG) of the Russian Academy of Sciences. Apatite aliquots (5–10 mg) were hand-picked under binoculars and then washed in an ultrasonic bath in Barnstead purified water and dissolved in 1N HCl at room temperature for a day. Plagioclase concentrate was separated in heavy liquids with subsequent hand picking of plagioclase monofraction under the binoculars. Then, plagioclase separate was ground in powder. The powdered plagioclase at first was leached in 0.5N HF for 0.5 h at room temperature, and then in concentrated (16N) HNO₃ for four hours at 70°C. Then, the sample was held at room temperature for 12 h and after removal of solution, was treated by concentrated (12N) HCl following the same scheme. Plagioclase leaching was conducted to remove the possible radiogenic Pb, which could be accumulated from trace U-bearing mineral inclusions, as well as from iron oxides (which could adsorb U). The leaching residue was decomposed by a mixture of concentrated HF and HNO₃.

Solutions obtained during decomposition of minerals were divided into two aliquots to determine: (1) U and Pb contents; (2) Pb isotope composition. The U and Pb concentrations were determined by isotope dilution using a mixed spike ²³⁵U + ²⁰⁸Pb. Lead was extracted using a Bio-Rad® anion-exchange resin in a bromide form following technique (Manhes et al., 1978), while uranium was extracted on an UTEVA SPEC extraction resin in a nitrate form. The lead isotope composition and Pb and U contents were measured on a Triton TI multicollector mass spectrometer. Laboratory blanks for Pb and U were no more than 0.05 and 0.005 ng, respectively. The measured Pb isotope ratios were corrected for fractionation coefficient established by multiple determination of Pb isotope composition in an SRM-982 standard and equal 0.13% per mass unit. Obtained raw isotope data were

processed and isochron parameters were calculated using ISOPLOT software (Ludwig, 2003). All errors listed in tables and used in calculations correspond to 2σ .

Prior to **Sm–Nd isotope analysis**, amphibole, titanite, and apatite monofractions were treated in 2.2 N HCl solution for 60 minutes to remove surface pollutions and supergene alterations and then were decomposed in an HF : HNO₃ : HClO₄ mixture in proportions 5 : 1 : 1 at 120°C for 24 h. Prior to the decomposition, samples were mixed with a mixed spike ¹⁴⁹Sm–¹⁵⁰Nd. After evaporation, the samples were treated in an HCl : HNO₃ mixture for 24 h in order to remove fluorides. Then, the samples were repeatedly evaporated and converted into hydrochloride form. Subsequent extraction of Sm and Nd was carried out on an Ln-Resin (Eichrom®) ion-exchange resin according to technique (Mikova and Denkova, 2007).

The Nd isotope composition was determined on a Triton TI multichannel solid-phase mass spectrometer. Thereby, the Sm and Nd concentrations and ¹⁴⁷Sm/¹⁴⁴Nd ratios were measured by isotope dilution. The reproducibility of Sm and Nd measurements in the BCR-1 standard accounted for $\pm 0.5\%$. Blanks were 0.3 ng for Sm and 0.5 ng for Nd. The measurement of BCR-1 standard (6 measurements) gave Sm = 6.47 ppm, Nd = 28.13 ppm, ¹⁴⁷Sm/¹⁴⁴Nd = 0.1380, ¹⁴³Nd/¹⁴⁴Nd = 0.512642 ± 14 . During the measurements, ¹⁴³Nd/¹⁴⁴Nd value in the JNdi-1 standard accounted for 0.512098 ± 8 (2σ , 12 measurements). The Nd isotope composition was adjusted to the certified JNdi-1 standard ¹⁴³Nd/¹⁴⁴Nd = 0.512117 (Tanaka et al., 2000).

The calculation of age based on the Sm–Nd whole-rock and mineral isotope data was carried out using an R-Isoplot software (Vermeesch, 2018). For calculations, the following relative errors for ¹⁴⁷Sm/¹⁴⁴Nd and ¹⁴³Nd/¹⁴⁴Nd were 0.5 and 0.005%, respectively.

Thermodynamic calculations of mineral formation were carried out using a MAGEMin software (Mineral Assemblage Gibbs Energy Minimizer) (Riel et al., 2022). This program is a Gibbs free energy minimization solver package, which computes the most stable mineral assemblage and melt for a given bulk rock composition, temperature, and pressure. The calculations also take into account oxygen fugacity, water content in the system, as well as possible assimilation and fractionation of the melt. Compared to other softwares aimed at constructing the pseudosections, MAGEMin offers an opportunity to calculate phase equilibria not only in metamorphic but also in magmatic systems. Magmatic mineral formation was calculated using thermodynamic database (Holland et al., 2018) updated by (Green et al., 2025). This database is applied for wide ranges of composition (from peridotite to granite), pressures (0.001–70 kbar), temperatures (from 650°C and higher to the liquidus temperature of peridotite) in the K₂O–Na₂O–CaO–FeO–MgO–Al₂O₃–SiO₂–H₂O–TiO₂–Fe₂O₃–Cr₂O₃ system.

Unlike other softwares (e.g., Perple_X, Connolly, 1990), this software was aimed at modeling magmatic process and employs the most accurate (at present day) thermodynamic database of given minerals, which, in particular, significantly improves modeling amphibole crystallization in the system.

Metamorphic transformations were calculated using database (Green et al., 2016), which was calibrated for metamafic rocks and applied in the Na₂O–CaO–K₂O–FeO–MgO–Al₂O₃–SiO₂–H₂O–TiO₂–Fe₂O₃ system for pressures no more than 13 kbar.

Results of microprobe analysis (EPMA) were processed in a MINAL software (Dolivo-Dobrovolsky, 2025) aimed at calculating the mineral formulas. Amphibole analyses were treated using software by (Locock, 2014) in compliance with the nomenclature recommended by the International Mineralogical Association (Hawthorne et al., 2012).

Photographs of thin sections were made by digital photocopiers (10–40X) mounted on Polam and Olympus optical microscopes and attached to a personal computer.

Lead isotope analysis was carried out for seven apatite monofractions and three feldspar monofractions (plagioclase, K-feldspar) from the rocks of the second intrusive phase, while Sm–Nd analysis was performed for bulk samples, two amphibole fractions, and two titanite fractions from host amphibolites.

GEOLOGICAL POSITION OF THE STUDIED SAMPLES AND MINERALOGICAL-PETROGRAPHIC CHARACTERISTICS

The Velimyaki massif is located in the Raahe–Ladoga suture zone of the Northern Ladoga region (Fig. 1), where it intrudes the Early Proterozoic sequences of the Sortavala and Ladoga groups (Ladoga..., 2020).

More comprehensive data on the structure and composition of massif are reported in the following publications (Saranchina, 1948; Alekseev, 2007; Baltybaev et al., 2010; 2024; Ladoga..., 2020, and others).

The massif contains pyroxenites, monzodiorites, and monzonites of different metamorphic grade from practically unaltered rocks that retained magmatic texture and minerals to highly recrystallized rocks (Fig. 2). Primary magmatic minerals in the rocks are clinopyroxene, brown hornblende, phlogopite, plagioclase, and magnetite. Metamorphic минералы are green hornblende, actinolite, and late plagioclase. Subordinate minerals are apatite and titanite.

The Rocks of the First Phase – Pyroxenites (B-22-537-1, B-22-550, B-22-551, B-22-552)

Unaltered or weakly altered pyroxenites (B-22-537-1) (Figs. 2a, 2b) are made up of subhedral clinopyroxene

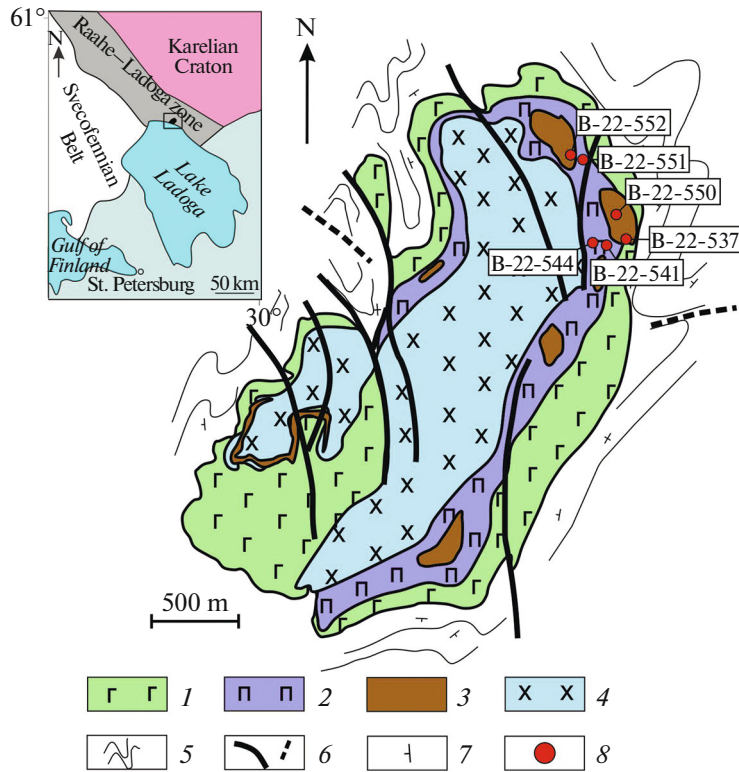


Fig. 1. Tectonic position and schematic geological map of the Velimiyaki massif (modified after Alekseev, 2008): (1) monzogabbro, monzodiorites of the second phase; (2) monzogabbro, monzodiorites of the second phase, intermediate zone; (3) bodies of clinopyroxenites and melanocratic monzogabbro of the first phase; (4) monzodiorites and monzonites of the second phase; (5) gneisses and schists of the Ladoga Group; (6) inferred and proved faults; (7) dip and strike; (8) sampling localities and their numbers. Box in the inset shows the position of the Velimiyaki massif in the geological structures of the southeastern Fennoscandian Shield.

(50–70 vol %) and anhedral grains of brownish, likely magmatic hornblende (7–40 vol %).

According to EPMA data, clinopyroxene is represented by diopside, $xMg = 0.87–0.69$ (Fig. 3a).

Brownish hornblende is represented by magnesiohastingsite and high-Ti magnesiohastingsite (Fig. 4a). Brownish hornblende also occurs as small xenomorphic inclusions in clinopyroxene grains.

Secondary amphiboles are formed after clinopyroxene during metamorphism. In weakly altered varieties (B-22-550), clinopyroxene (around 40 vol %) is surrounded by green hornblende rims. According to EPMA data, green hornblende from the rocks of the first phase is represented by hastingsite, potassium hastingsite, and ferrihornblende (Fig. 4a). In the more altered rocks (B-22-552) (Figs. 2c, 2d), clinopyroxenes are almost completely replaced by pseudomorphs with central parts filled with actinolite (up to 70 vol %) and rims made up of green hornblende (up to 20 vol %) (Fig. 6c). The green hornblende also fills interstices between pseudomorphs. Amphiboles rims of the pseudomorphs contain potassium admixture (K_2O content on average is 1.5 wt %). These amphiboles also usually contain chlorine admixture (on average, 0.28 wt %).

Brownish biotite appears together with green hornblende (1–20 vol %). According to EPMA data, biotite in the rocks of the first phase is represented by phlogopite with weakly varying tetrahedral aluminum from 1.1 to 1.3 apfu (Fig. 4b). It usually contains titanium admixture amounting 1.4–2.7 wt %, as well as insignificant admixture of chlorine (up to 0.29 wt %).

Magnetite (7–20 vol %) forms equant round grains confined to the clinopyroxene crystals, ilmenite forms droplets in magnetite grains or exsolution lamellae (Fig. 6a). Magnetite and ilmenite grains could be also surrounded by thin titanite rim.

Apatite forms round, more rarely elongated prismatic grains. According to EPMA data, apatite in the rocks of the first phase is represented by hydroxyl-fluorapatite (Fig. 5), with insignificant admixture of chlorine (up to 0.36 wt %). Apatite is usually confined to the aggregates of green hornblende and biotite. Titanite segregations are frequently observed directly on the boundary of apatite crystals enclosed in biotite. They are likely formed due to the interaction of apatite with biotite, with input of titanium from biotite and calcium from apatite (Fig. 6e). In addition, allanite grains are observed near apatite grains. They are likely

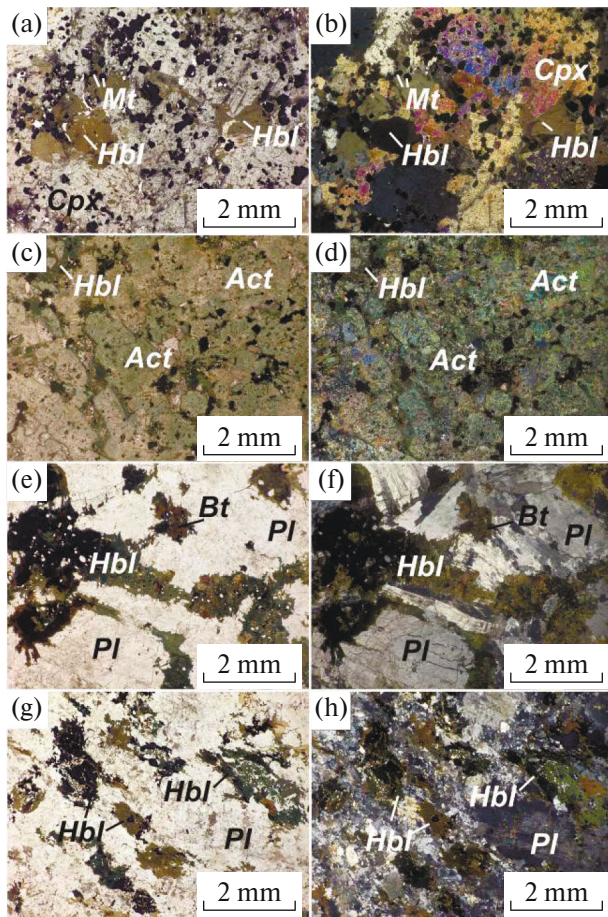


Fig. 2. Photographs of thin sections of main rock types of the Velimyki massif. First phase: (a, b) unaltered pyroxenite (sample B-22-537-1); (c, d) strongly altered pyroxenite with preserved magmatic texture (sample B-22-552). The second phase: (e, f) monzodiorite (sample B-22-541-1); (g, h) monzonite (sample B-21-478). Images under parallel (a, c, e, g,) and crossed (b, d, f, h) polarizers. Hereinafter, mineral abbreviations are given according to (Whitney and Evans, 2010).

formed through recrystallization of the earlier REE-enriched apatite.

With increase of plagioclase and sometimes K-feldspar contents (up to 50 vol % in total), pyroxenites grade into monzogabbro (B-22-552-1). The composition of plagioclase in the monzogabbro varies from andesine to oligoclase An_{40-13} (Fig. 3b). The most calcic plagioclase likely is of magmatic origin, while the most sodic plagioclases were formed during metamorphism. The monzogabbro also contains high-temperature perthite K-feldspar.

No relicts of magmatic minerals and magmatic textures are present in the **recrystallized monzogabbros** (B-22-551). These rocks are composed of the large xenomorphic grains of green hornblende sometimes intergrown with actinolite (in total, around 40 vol %) and brownish biotite (40 vol %). Sometimes, these rocks contain carbonate (up to 10 vol %) as well as magnetite (5 vol %) and apatite (1 vol %).

Rocks of the Second Phase—Monzodiorites (B-22-541, B-22-544) and Monzonites (B-21-478, B-22-546)

The monzodiorites (Figs. 2e, 2f) are composed of plagioclase (50–70 vol %), green hornblende and actinolite (10–20 vol %), and biotite (10–20 vol %). Subordinate minerals are apatite (5 vol %) and magnetite (1 vol %).

Plagioclase usually forms large elongated prismatic crystals with thin twinning. Some crystals frequently contain segments that lost twinning and acquired blocky extinction. Crystal rims are frequently subjected to granulation and oxidation (Fig. 6b). According to EPMA data, plagioclase in the rocks of the second phase varies from labradorite An_{56} (in the cores) to albite An_6 (rims at the contact with hornblende) (Fig. 3b).

Amphiboles in the freshest rocks form actinolite–hornblende pseudomorphs after clinopyroxene,

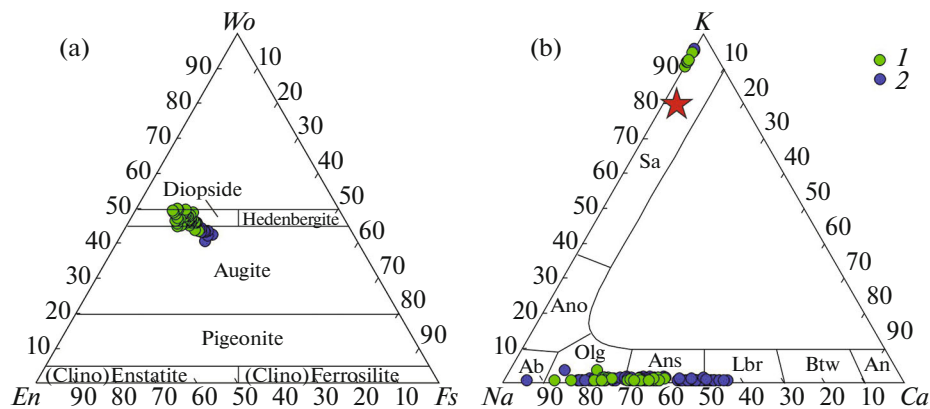


Fig. 3. Compositions of (a) clinopyroxenes and (b) feldspars from the rocks of the Velimyki massif: (1) first phase, (2) second phase. Asterisk shows integrated composition of perthitic K-feldspar from monzogabbro, first intrusive phase (B-22-552-1).

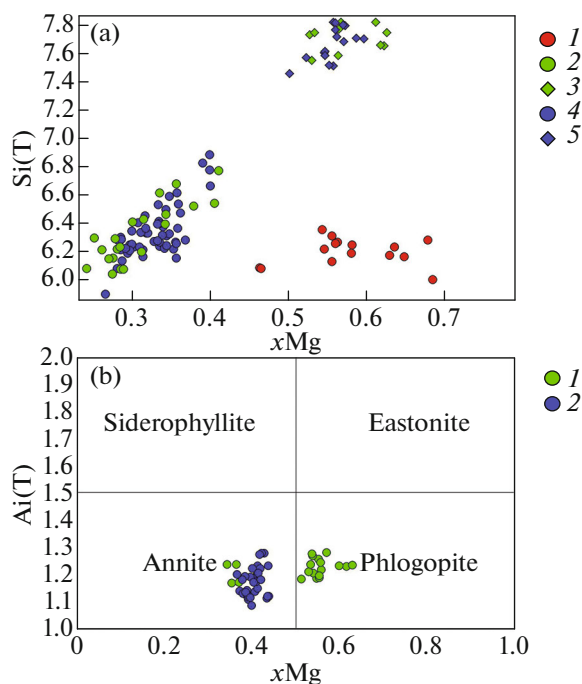


Fig. 4. Compositions of (a) amphiboles and (b) biotites from the rocks of the Velimiyaki massif. (a): (1) brown titanium amphiboles with elevated Mg#, supposedly magmatic; (2) green hornblendes from the rocks of the first phase; (3) actinolites from the rocks of the 1st phase; (4) green hornblende of the rocks of the second phase; (5) actinolites from the rocks of the second phase. (b): (1) biotites from the rocks of the first phase; (2) biotites from rocks of the second phase.

which are similar to those of pyroxenites. Central parts of such pseudomorphs rarely contain clinopyroxene relicts. Clinopyroxene in these rocks is represented by augite, which has lower Ca and higher Fe ($xMg = 0.67\text{--}0.61$) composition compared to clinopyroxene from pyroxenites ($xMg = 0.87\text{--}0.69$) (Fig. 3a). Green hornblende is practically identical in composition to the hornblende from the first phase (Fig. 4a). In the more altered rocks, actinolite cores in the pseudomorphs are replaced by symplectite-like aggregate of hornblende and quartz (Fig. 6d). In the more altered rocks, pseudomorphs are replaced by intergrowths of subhedral green hornblende and biotite, which sometimes contain fragments of amphibole–quartz aggregates.

Biotite occurs in intergrowths with green hornblende or forms own large subhedral or anhedral grains. Biotite in the rocks of the second phase is represented by annite, which has higher Fe composition compared to the biotite of the first phase (Fig. 4b).

Apatite in this phase, as in pyroxenites, forms round or elongate-prismatic grains, aggregates of which are confined to the green hornblende and biotite. In composition, apatite from the rock of the second phase is identical to the apatite from the first phase (Fig. 5).

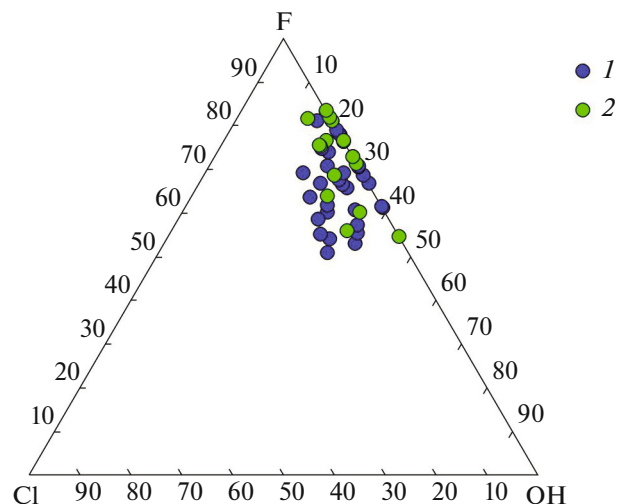


Fig. 5. Content of volatile components in the apatite from rocks of the Velimiyaki massif: (1) rocks of the first phase, (2) rocks of the second phase.

The monzonites (Figs. 2g, 2h) differ from monzodiorites in the greater content of plagioclase. Small anhedral K-feldspar with microcline hatching is observed among granulated plagioclase crystals. The least altered rocks showing no granulation have primary ophitic texture—plagioclase is more euhedral compared to clinopyroxene (more exactly, actinolite–hornblende pseudomorphs after it). Such more preserved rocks are devoid of K-feldspar. The relationships of mafic minerals, as well as apatite, are the same as in the monzodiorites.

U–Pb SYSTEM OF APATITE

Obtained data on different apatite samples in the diagram $^{206}\text{Pb}/^{204}\text{Pb}$ – $^{207}\text{Pb}/^{204}\text{Pb}$ fall within a range of 1805–1812 Ma (Fig. 7, Table 1). Slightly older age of 1812 Ma was obtained on apatite from sample B22–541 compared to the relatively younger age value of 1805 Ma for apatite from sample B22–544 (Figs. 7a, 7b). However, these differences likely are insignificant, since obtained results are identical within errors.

These age values agree well with U–Pb ages of the same apatites. In particular, apatite from sample B22–541 defined a concordant U–Pb age of 1810 ± 3 Ma (Fig. 8a). Thereby, data points of isotope compositions of apatite from sample B22–544 seemed to be above the concordia line in the U–Pb diagram (Fig. 8b). A reverse discordance (when $t(^{207}\text{Pb}/^{206}\text{Pb}) < t(^{207}\text{Pb}/^{235}\text{U}) < t(^{206}\text{Pb}/^{238}\text{U})$) is typical of phosphates, in particular, of apatite (Shukolyukov et al., 1974). Discordia determined by these points defines an upper intercept age of apatite at 1789 ± 12 Ma, which within error coincides with the age of this apatite obtained in the Pb–Pb diagram and with U–Pb age of apatite from the first sample. The great error in the lower intercept age makes it impossible to date the later superimposed event.

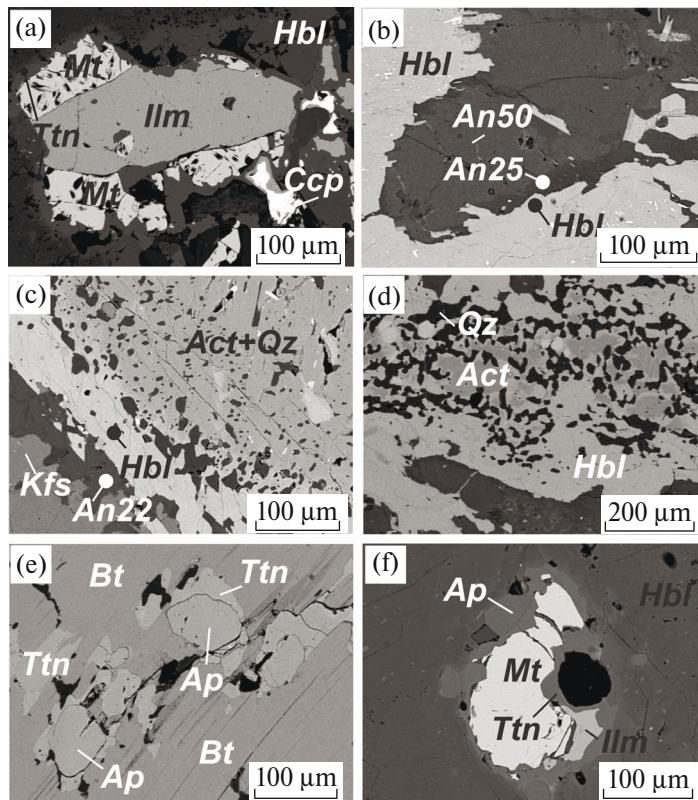


Fig. 6. BSE-images of minerals from the Velimyaki massif: (a) intergrowths of magnetite with ilmenite and thin titanite rim around them; intergrowths are enclosed in the hornblende; (b) crystal of magmatic plagioclase with metamorphic rim of more acid composition. Circles show analytical spots of plagioclase and hornblende, for which equilibrium temperature is estimated at 655°C (Holland and Blundy, 1994); (c) hornblende–actinolite pseudomorphs after clinopyroxene. Circles show analytical points of plagioclase and hornblende with equilibrium temperature estimated at 665°C (Holland and Blundy, 1994); (d) quartz–hornblende pseudomorph after clinopyroxene with actinolite relicts; (e) development of titanite at the contact of apatite and biotite; (f) later titanite and likely, late apatite around primary magmatic magnetite and ilmenite enclosed into hornblende crystal.

Sm–Nd TITANITE SYSTEM

We studied titanites from framework rocks–amphibolites of the Sortavala Group, which are intruded by gabbroids of the Velimyaki massif. The formation of these titanites is unambiguously related to the regional metamorphism superimposed onto both the framework rocks and Velimyaki massif.

Sm–Nd system of titanite, as that of metamorphic amphibole, with sufficiently high error, gives the metamorphic age of 1.84–1.82 Ga (Fig. 9, Table 2). These age estimates are consistent with U–Pb and Rb–Sr dates on other metamorphic minerals and rocks (Baltysbaev et al., 2024a).

CONDITIONS OF FORMATION AND TRANSFORMATION OF APATITE-BEARING ROCKS: EVIDENCE FROM THERMOBAROMETRIC DATA AND MODELING OF MINERAL FORMATION

The peculiarities of mineral formation were determined by modeling magmatic crystallization of the

initial melt of the Velimyaki massif. It should be noted that the rocks of the first phase (clinopyroxenite and melanocratic monzogabbros) form lenticular bodies in the intermediate zone of the massif. These bodies were mapped in detail by Alekseev (Fig. 1; Alekseev, 2008), the area of their outcrops at the present-day erosion level is around 10%. On this basis, the initial melt of the massif was calculated. It was calculated by the following way: (a) compositions of rocks of the first phase (pyroxenites, monzogabbros, 15 analyses) and rocks of the second phase (monzodiorites and monzonites, 25 analyses) were averaged, (b) the averaged compositions of the first and second phases were mixed in the following proportions: (a)—10 to 90%, (b) 20 to 80%, (c) 30 to 70%, respectively.

These three possible compositions of initial melt were used for further modeling. Above presented proportions were determined from phase proportions at the observed (mapped) modern erosion section, with allowance for the fact that the volume of rocks of the first phase at the depth is more than at the surface (20 and 30%). The existing data make it impossible to determine reliably the proportions of pyroxenites and

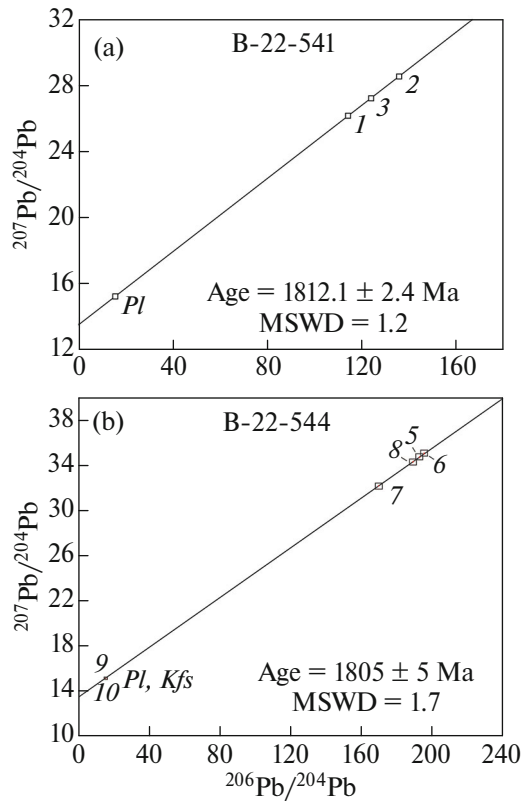


Fig. 7. Pb–Pb isochron for apatite from the rocks of the second phase of the Velimyaki massif. (a) sample B-22-541 (monzodiorite), (b) sample B22-544 (monzodiorite).

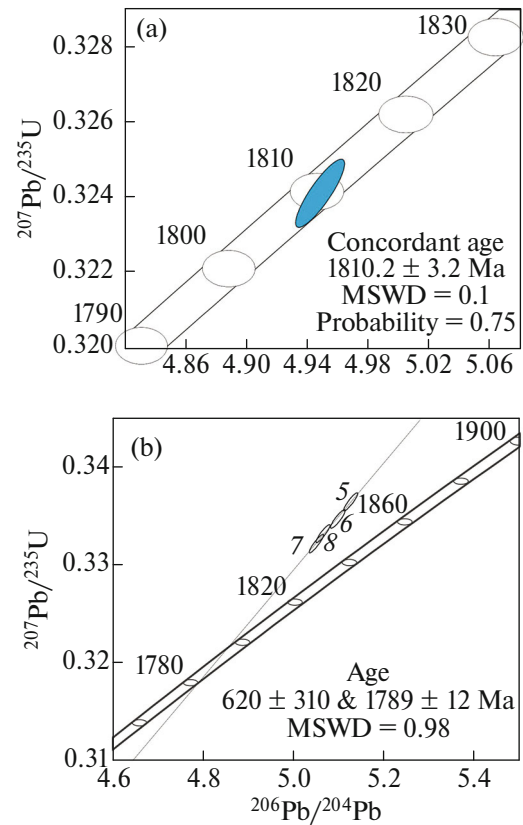


Fig. 8. U–Pb diagram for apatite from the rocks of the second phase of the Velimyaki massif. (a) sample B-22-541 (monzodiorite), (b) sample B22-544 (monzodiorite).

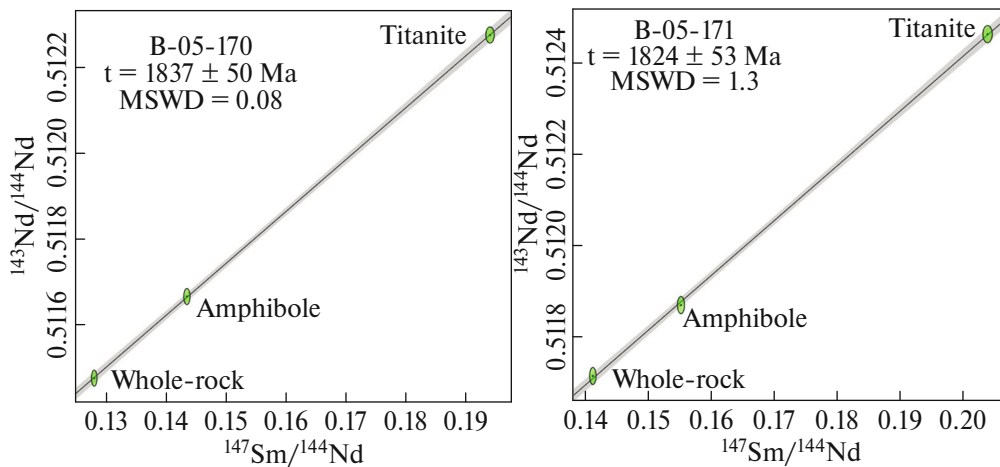


Fig. 9. Sm–Nd isochron for titanites from amphibolites.

monzogabbros in the outcrops of the first phase and monzodiorites and monzonites in the second phase. Therefore, their proportions were ignored during calculation of composition of the initial melt.

In modeling, the pressure in the chamber was taken equal 400 MPa, which corresponds to values estimated using mineral geobarometers of surrounding rocks (Baltybaev et al., 2000).

The water content in the melt and oxygen fugacity were determined by numerical modeling. In particular, modeling at water content less than 3 wt % gives orthopyroxene, which is absent in the massif rocks. Based on these data, modeling was performed for the melt with water content of 3 wt % (or more).

The oxygen fugacity was given by QFM + 2 buffer, because more reducing conditions suppress crystalli-

Table 1. Pb isotope composition of apatite and feldspars from the rocks of the second phase of the Velimiyaki massif

Ordinal no.	Sample no./ mineral	$^{206}\text{Pb}/^{204}\text{Pb}$	$^{207}\text{Pb}/^{204}\text{Pb}$	$\frac{^{208}\text{Pb}}{^{204}\text{Pb}}$	$^{207}\text{Pb}/^{235}\text{U}$	$^{206}\text{Pb}/^{235}\text{U}$	Age, Ma		
							$^{206}\text{Pb}/^{235}\text{U}$	$^{207}\text{Pb}/^{235}\text{U}$	$^{207}\text{Pb}/^{206}\text{Pb}$
1	541-Ap	114.12	26.177	92.158	—	—	—	—	—
2	541-Ap	135.72	28.553	104.36	4.947 ± 0.013	0.3241 ± 0.0007	1809.8 ± 4.1	1810.4 ± 4.8	1811.1 ± 2.4
3	541-Ap	123.91	27.241	97.917	5.133 ± 0.014	0.3364 ± 0.0008	1869.3 ± 4.3	1841 ± 5.1	1810.4 ± 2.7
4	541-Pl	$15.574 (15.524)$	$15.246 (15.240)$	35.155	—	—	—	—	—
5	544-Ap	195.61	35.119	117.72	5.125 ± 0.013	0.3365 ± 0.0008	1869.9 ± 4.2	1840.3 ± 4.6	1807 ± 1.8
6	544-Ap	193.01	34.79	117.33	5.050 ± 0.013	0.3323 ± 0.0008	1849.3 ± 4.3	1827.7 ± 4.7	1803.2 ± 1.8
7	544-Ap	169.78	32.26	106.83	5.097 ± 0.013	0.3348 ± 0.0008	1861.5 ± 4.3	1835.6 ± 4.8	1806.5 ± 2.1
8	544-Ap	189.33	34.381	114.66	5.064 ± 0.013	0.3333 ± 0.0008	1854.2 ± 4.2	1830.2 ± 4.6	1802.9 ± 1.8
9	544-Kfs	$15.438 (15.420)$	$15.207 (15.205)$	35.008	—	—	—	—	—
10	544-Pl	$15.489 (15.432)$	$15.222 (15.216)$	35.07	—	—	—	—	—

The table reports isotope ratios corrected for the fractionation coefficient and blank. The Pb content varies from 7.91 to 9.21 ppm in apatite B22-541, and from 10.9 to 14.1 ppm in apatite B22-544. The U content is 11.8–14.7 ppm in apatite B22-541 and 19.4–25.3 ppm in B22-544. Feldspars in parentheses show isotope values of lead corrected for U decay at 1890 Ma (with allowance for correction, the lead isotope composition of feldspars at an age of 1.80 Ga, this does not affect the calculated age of apatite).

Table 2. Sm–Nd isotope composition of titanite from amphibolites

Sample no.	Mineral/ rock	Sm, ppm	Nd, ppm	$^{147}\text{Sm}/^{144}\text{Nd}$	$^{143}\text{Nd}/^{144}\text{Nd}$	$\pm 2\sigma^*$
B-05-170	Titanite	156.50	487.00	0.1942	0.512276	3
	Amphibole	8.24	34.69	0.1435	0.511667	4
	Whole rock	3.83	18.08	0.1280	0.511477	8
B-05-171	Titanite	103.70	307.50	0.2038	0.512463	1
	Amphibole	4.34	16.92	0.1551	0.511871	3
	Whole rock	2.91	12.45	0.1411	0.511716	3

* Measurement errors (standard error, absolute value) are given in the last digit.

zation of magnetite, content of which in the rocks of the first phase exceeds 10 vol %.

Modeling was made for equilibrium and fractional crystallization (Fig. 10).

Melt composition obtained by mixing of 10% average first phase and 90% average second phase yields the early crystallization of plagioclase both for equilibrium and fractional crystallization, which is not consistent with mineral phases observed in the massif rocks (Figs 10a, 10b).

Modeling with initial melt obtained by mixing of two phases in proportions of 20 and 80 and 30 and 70%, yields result, which fit well the observed crystallization sequence: early crystallization of clinopyroxene and magnetite is replaced by the crystallization of plagioclase and clinopyroxene (Figs. 10c, 10d, 10e, 10f). Thereby, at equilibrium crystallization, magnetite continues to form at the late stages, whereas fractional crystallization provides magnetite formation only at the early stage (prior to the appearance of magmatic

amphibole). Crystallization of magnetite mainly at the early stage is well consistent with natural data: ore bearing rocks are pyroxenites, whereas plagioclase rocks of the massif already do not contain significant amounts of magnetite.

Further temperature decrease at the late stage is associated with simultaneous crystallization of clinopyroxene and magmatic amphibole, which later give way to biotite and, for fractional crystallization, to K-feldspar. All these minerals are present in the massif and peculiarities of their formation will be discussed below.

For modeling of metamorphic mineral formation, *PT*-diagrams were plotted for most typical rocks of the first and second phases (pyroxenite, sample B-22-552, and monzodiorite, sample B-22-544) (Fig. 11). The water content in the system was taken to be 3 wt %, which provided modal content of minerals close to the observed one.

Phase diagram calculated for pyroxenite (Fig. 11a) is well consistent with observed metamorphic mineral assemblages. In particular, high-temperature field contains clinopyroxene–hornblende assemblage; clinopyroxene disappears with decreasing temperature, and further decrease leads to the actinolite formation. It is seen in thin sections that clinopyroxene is subsequently replaced by actinolite and hornblende, which indicates a change of relatively low-temperature by the higher temperature metamorphic stage. Obtained mineral assemblages show no strong dependence on pressure; and only low-pressure region is characterized by the appearance of insignificant amounts of plagioclase.

Modeling of metamorphic assemblage for rocks of the second phase encountered some difficulties (Fig. 11b). For instance, modeling demonstrates the biotite predominance over hornblende/actinolite, although studied rocks, in contrast, show opposite relations. This is explained by the incomplete correspondence of rock compositions to the database for metamafic rocks, in particular, due to the elevated alkalinity and higher silicity. Nevertheless, the higher temperature hornblende-bearing field and the lower temperature amphibole-free field could be distinguished in the *PT*-diagram. The actinolite field is confined to the medium-temperature low-pressure region, but at certain oxygen fugacities, it reaches 400 MPa, which corresponds

Table 3. Model compositions of an initial melt of the Velimyaki massif

Oxide	Av-10%	Av-20%	Av-30%
SiO ₂	52.58	51.50	50.45
Al ₂ O ₃	17.75	16.80	15.88
TiO ₂	0.94	1.08	1.22
FeO	9.38	10.33	11.26
MgO	3.75	4.57	5.37
MnO	0.17	0.18	0.19
CaO	7.27	7.86	8.44
Na ₂ O	3.83	3.52	3.23
K ₂ O	2.92	2.75	2.59
P ₂ O ₅	0.40	0.38	0.36
H ₂ O	1.01	1.01	1.00
Total	100	100	100

Compositions Av-10%, Av-20%, Av-30% correspond to mixing of the first and second phases in the following proportions: (a) 10 to 90%; (b) 20 to 80%, (c) 30 to 70%, respectively.

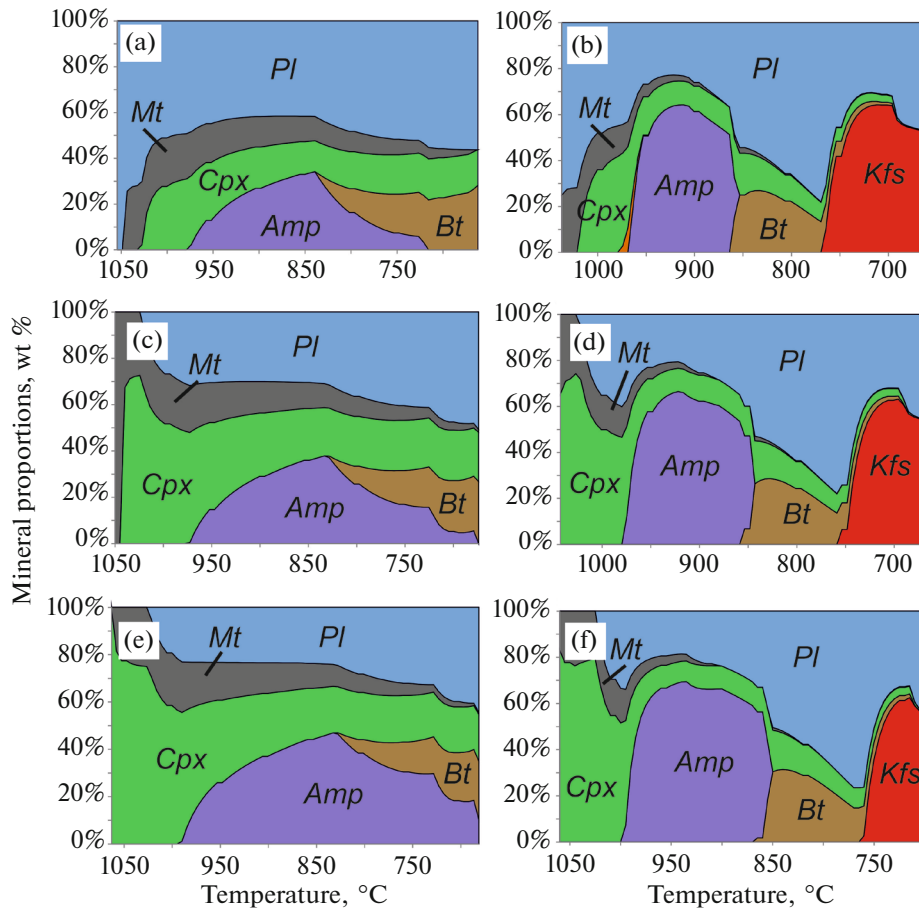


Fig. 10. Equilibrium and fractional crystallization of model initial melt. Equilibrium crystallization—left column, figures (a, c, e); fractional crystallization—right column (b, d, f). The composition of initial melt was calculated using following proportions of rocks of the first and second phases: (a), (b) 10 and 90%, (c), (d) 20 and 80%, (e), (f) 30 and 70%, respectively.

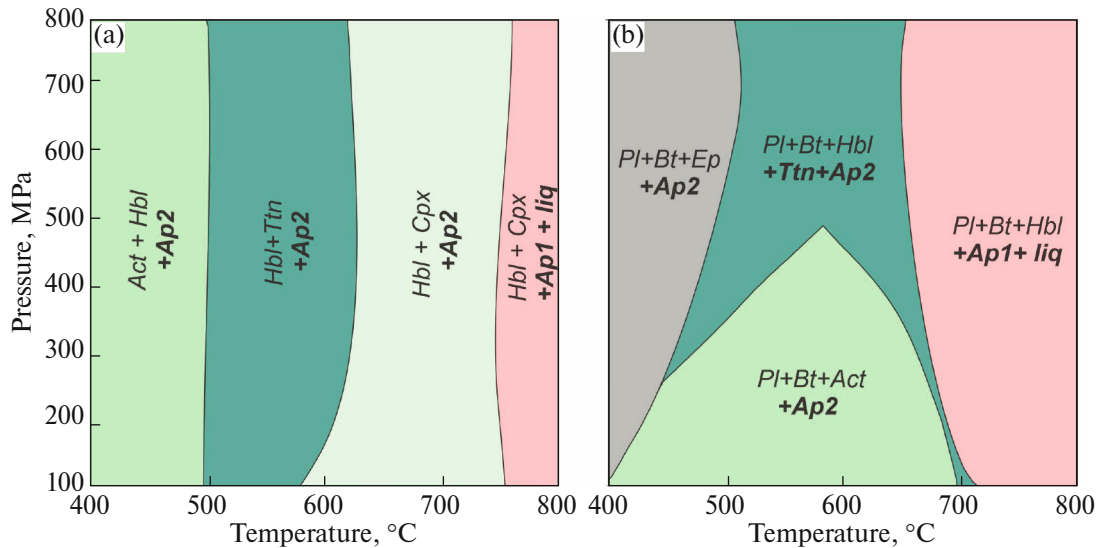


Fig. 11. Calculated *PT*-diagrams for (a) pyroxenite and (b) monzodiorite showing the stability fields of hornblende and actinolite mineral assemblages during metamorphism of these rocks. Additionally shown are apatite and titanite in these assemblages, appearance of which is inferred from petrographic observations (Fig. 12).

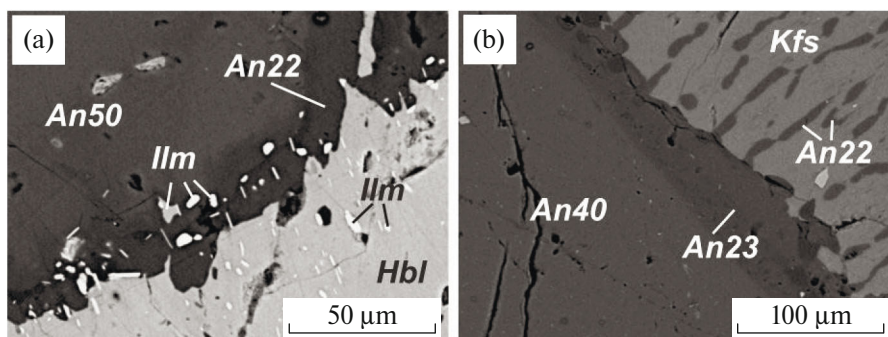


Fig. 12. BSE-images of green hornblende with inclusions of ilmenite (a) and perthitic K-feldspar (b) in the rocks of the Velimyaki massif. It is suggested that these compositions and structures of minerals demonstrate postmagmatic alterations of minerals initially formed from the melt.

to the pressure of metamorphic mineral formation both in the region, and in the massif rocks, in particular (Baltybaev et al., 2024).

DISCUSSION

Modeling of Equilibrium and Fractional Crystallization and Correspondence of Results to the Natural Data

Modeling of magmatic crystallization agrees well with natural data and confirms the opportunity of the formation of differentiated rocks of the massif from a common melt: plagioclase-free $Cpx + Mt$ assemblage (analogue of the first phase rocks) is simulated at the early stages of crystallization and then gives way to the essentially plagioclase rocks (analogue of the second phase). Thereby, ore-bearing (magnetite) rocks are pyroxenites, not plagioclase rocks, which is well consistent with the model of fractional crystallization. At equilibrium crystallization, magnetite is formed uninterruptedly within the entire temperature interval. This fact, as well as the absence of signs of resorption and the replacement of early magmatic minerals by later ones (excluding metamorphic actinolite and green hornblendes from consideration) are more prone to fractional rather than equilibrium crystallization. Observations are also consistent with the joint crystallization of clinopyroxene and magmatic amphibole at the later stage, which were subsequently replaced by biotite and K-feldspar assemblages (Fig. 10). The model of fractional crystallization of rock-forming minerals is well consistent with natural data and confirms the possible formation of differentiated rocks of the massif from a common melt.

The magmatic Ti-rich hornblende is observed only in pyroxenites, and is absent in the rocks of the second phase. The latter, instead contains green hornblende with ilmenite exsolution lamellae (Fig. 12a). Thereby, such hornblende always forms independent crystals and is not observed in pseudomorphs after clinopyroxene. The green hornblende could be formed after earlier Ti-rich magmatic amphibole with release of tita-

nium as ilmenite phase. The later stage of amphibole recrystallization is also supported by the acidification of associated plagioclase up to An_{22} , whereas its central part retains more sodic composition, around An_{50} (Fig. 12a).

Biotite frequently occurs both in the pyroxenites of the first phase and in the rocks of the second phase. Temperature of its formation determined using Ti-biotite thermometer corresponds to the metamorphic stage (Baltybaev et al., 2024), however, similar metamorphic biotite could be formed after earlier magmatic biotite.

At the final stage of crystallization, biotite is replaced by K-feldspar. The nature of this mineral is controversial: some researchers suggest its magmatic origin (Saranchina, 1948), while others are prone to the metasomatic formation (Alekseev and Kotova, 2010). The presence of high-temperature perthite K-feldspar in the massif rocks (Fig. 12b) points to its magmatic nature, which is consistent with modeling results: at the late stage of fractional crystallization, biotite gives way to the K-feldspar even at high water content in the system (more than 3 wt %). This is likely related to the increasing fraction of potassium in a residual melt.

Relationships of Apatite with Other Minerals

Given the presence of magmatic and metamorphic mineral assemblages in the studied metagabbroids, special attention should be given to the relations of apatite with other minerals. It was noted that apatite is frequently intergrown with metamorphic minerals such as green hornblende and actinolite, biotite, titanite, and quartz (Figs. 13a–13d). In the PT -diagram, these minerals occupy the medium- and low-temperature regions, while their stability field does not depend significantly on pressure (Figs. 11a, 11b).

Given peculiar association of apatite with metamorphic minerals, as well as its much younger Pb–Pb age compared to the intrusion age, the observed apatite grains were formed by its complete recrystalliza-

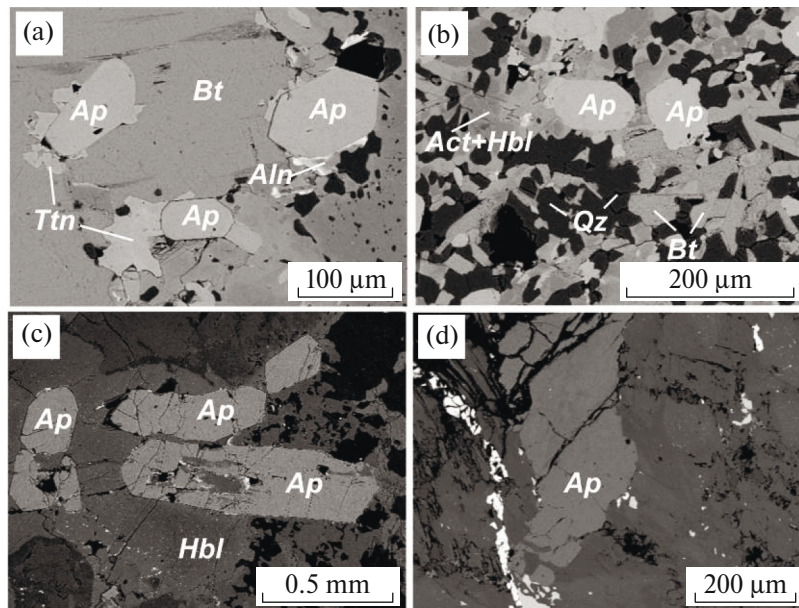


Fig. 13. BSE images of apatite grains in the rocks of the Velimyaki massif. Apatite is confined to the development zones of secondary (metamorphic) minerals: (a) apatite in biotite in the intergrowths with late titanite (monzodiorite, sample B-22-544); (b) in the actinolite–hornblende–quartz matrix from the center of pseudomorph after clinopyroxene (monzodiorite, sample B-22-544); (c) apatite grain in the hornblende porphyroblast (pyroxenite, sample B-22-550); (d) deformed apatite grain (pyroxenite, sample 6v2003).

tion during superimposed metamorphism. Such apatite could be also newly formed rather than recrystallized at the expense of previously existing minerals. However, this is more complex and, hence, less probable model, which poorly agrees with observed paragenetic relationships of apatite with other minerals in the rock.

Isotope Age of Apatite and Titanite

Obtained Pb–Pb and U–Pb ages of apatite (1.80–1.81 Ga) from monzodiorites of the second phase of the Velimyaki massif indicate a time gap of 60–70 Ma from a moment of magmatic crystallization, since the U–Pb zircon age of the intrusion is 1.89 Ga (Alekseev, 2008; Alekseev and Kotova, 2010). Such age rejuvenation of apatite is likely related to the high sensitivity of U–Pb systematics of this mineral to the superimposed events (metamorphism and hydrothermal processes), which allows easy recrystallization of apatite with resetting of its U–Pb system.

Relatively low closure temperature of U–Pb apatite system (~450–550°C), which could be lower in the deformed and hydrothermally altered samples, provides obtaining the younger U–Pb (Pb–Pb) apatite ages (Kärkkäinen and Appelqvist, 1999; Cochrane et al., 2014; Kirkland et al., 2018; O’Sullivan et al., 2020; Chew and Spikings, 2021, and others).

Thus, U–Pb isotope system in apatite not always records the time of magmatic crystallization, because apatite isotope system is sensitive to secondary pro-

cesses. The studies of apatite from the rocks of the second phase of the Velimyaki massif demonstrate such sensitivity to the superimposed metamorphic events. The development area of this massif was spanned by pervasive Late Svecofennian events (Baltybaev et al., 2024a), which is consistent with obtained differing apatite ages. These ages are grouped into the interval of postmagmatic stage of 1.84–1.79 Ga, but each value is related to the definite episode of metamorphic mineral formation.

Sm–Nd age of titanite from host amphibolites unambiguously could be related to its crystallization during regional metamorphism, which overprinted both the framework rocks and the rocks of the Velimyaki massif.

CONCLUSIONS

The mineralogical-petrographic and thermodynamic modeling can be used to reconstruct the history of formation of the rocks of the Velimyaki massif and their transformations during metamorphism. The rocks of the first and second phases were likely formed from a single parent melt by fractional crystallization. The early stage was responsible for the crystallization of clinopyroxene and titanomagnetite, which are followed by plagioclase, magmatic Ti-rich hornblende, and biotite. Magmatic K-feldspar was likely formed at the final stage.

Metamorphism causes the recrystallization of primary magmatic minerals. Two metamorphic stages

can be proposed. At the first stage (around 500°C), clinopyroxene is replaced by actinolite aggregate. At the second, higher temperature (650–750°C) stage, actinolite pseudomorphs are surrounded by a rim of metamorphic green hornblende, which gradually replaces actinolite up to the formation of quartz–hornblende aggregates. The formation of green hornblende is accompanied by the recrystallization of biotite. Metamorphism was also responsible for the formation of acid plagioclase, secondary K-feldspar, and titanomagnetite exsolution into magnetite and ilmenite lamella, and formation of titanite.

Apatite from the second phase of the Velimyaki massif is intergrown with metamorphic minerals such as green hornblende and actinolite, acid plagioclase, titanite, and quartz. The paragenesis of apatite with metamorphic minerals in combination with its much younger Pb–Pb (1812 ± 2 and 1805 ± 5 Ma) and U–Pb (1810 ± 3 Ma) ages compared to the age of the intrusion (1894 ± 6 Ma) indicate the recrystallization of this mineral during superimposed metamorphism.

Timing of regional metamorphism estimated using Sm–Nd method on titanite from host amphibolites with large error corresponds to the postmagmatic stage of transformations at 1.84–1.82 Ga.

The high sensitivity of the U–Pb apatite system to the superimposed metamorphic events makes it possible to identify the influence of the Late Svecofennian regional metamorphism on the intrusion.

ACKNOWLEDGMENTS

We are grateful to reviewers, A.V. Girnis (Institute of Geology of Ore Deposits, Petrography, Mineralogy, and Geochemistry, Russian Academy of Sciences) and T.V. Kaulina (Kola Science Center, Russian Academy of Sciences), for valuable comments that significantly improved this work.

FUNDING

This work was carried out using facilities of the Shared Equipment Center “AIRES” (Institute of Precambrian Geology and Geochronology, Russian Academy of Sciences, St. Petersburg).

The work was made in the framework of the Assignment Task of the Institute of Precambrian Geology and Geochronology, Russian Academy of Sciences (project no. FMUW-2026-0006)

CONFLICT OF INTEREST

The authors of this work declare that they have no conflicts of interest

REFERENCES

- I. A. Alekseev, *Candidate's Dissertation in Geology and Mineralogy* (St-Petersb. Gos. Univ., St. Petersburg, 2008).
- I. A. Alekseev and I. K. Kotova, “Geological structure and ore potential of the Velimyaki Massif (Northern Ladoga Region),” in *Proc. Youth Scientists of the IPGG RAS*, Ed. by V. S. Abushkevich and N. A. Alfimova (St. Petersburg, 2010), pp. 47–82.
- Sh. K. Baltybaev, V. A. Glebovitskii, I. V. Kozyreva, D. L. Konopel'ko, O. A. Levchenkov, I. S. Sedova, and V. I. Shuldiner, *Geology and petrology of the Ladoga Svecofennides*, Ed. by V. A. Glebovitskii (St. Petersburg. Gos. Univ., St. Petersburg, 2000).
- Sh. K. Baltybaev, V. M. Savatenkov, and M. E. Petrakova, “T-t evolution of the Early Proterozoic rocks in the Northern Ladoga region from the data on U–Pb, Rb–Sr and Sm–Nd systems in minerals,” *Geodynam. Tectonophys.* **15** (3), 759 (2024a).
- Sh. K. Baltybaev, R. L. Anisimov, I. M. Vasilyeva, N. G. Rizvanova, O. L. Galankina, and V. M. Savatenkov, “Ore apatite-bearing mineralization of the Velimyaki gabbroid massif in the Raahe–Ladoga zone of the Northern Ladoga region: Identification of formation conditions and estimation of apatite age,” *Geochem. Int* **62** (11), 1137–1154 (2024b).
- V. A. Bogachev, V. V. Ivanikov, I. V. Kozyreva, D. L. Konopel'ko, O. A. Levchenkov, and V. I. Shul'diner, “U–Pb zircon dating of synorogenic gabbro-diorite and granitoid intrusions of the Northern Ladoga region,” *Vestn. SPbGU. Ser 7* (3), 23–33 (1999).
- A. E. Boudreau, E. A. Mathez, and I. S. Mccallum, “Halogen geochemistry of the Stillwater and Bushveld complexes: evidence for transport of the platinum-group elements by Cl-rich fluids,” *J. Petrol.* **27**, 967–986 (1986).
- D. M. Chew and R. A. Spikings, “Apatite U-Pb thermochronology: A review,” *Minerals* **11** (10), 1095 (1095). <https://doi.org/10.3390/min11101095>
- R. Cochrane, R. A. Spiking, D. Chew, J.-F. Wotzlaw, M. Chiaradia, S. Tyrrell, U. Schaltegger, and R. Van Der Lelij, “High temperature (>350°C) thermochronology and mechanisms of Pb loss in apatite,” *Geochim. Cosmochim. Acta* **127**, 39–56 (2014).
- J. A. Connolly, “Multivariable phase-diagrams—an algorithm based on generalized thermodynamics,” *Amer. J. Sci* **290**, 666–718 (1990).
- D. V. Dolivo-Dobrovol'skii, “MINAL—a program for efficient work with chemical analysis of minerals,” *Zap. Ross. Mineral. O-va* **154** (1), 142–150 (2025).
- E. C. R. Green, R. W. White, J. F. A. Diener, R. Powell, T. J. B. Holland, and R. M. Palin, “Activity–composition relations for the calculation of partial melting equilibria in metabasic rocks,” *J. Metamorph. Geol.* **34** (9), 845–869 (2016).
- E. C. R. Green, T. J. B. Holland, R. Powell, O. M. Weller, and N. Riel, “Corrigendum to: Melting of peridotites through to granites: A Simple thermodynamic model in the system KNCFMASHTOCr, and, a thermodynamic model for the subsolidus evolution and melting of peridotite,” *J. Petrol.* **66** (1), egae079 (2025).
- D. E. Harlov, “Apatite: A fingerprint for metasomatic processes,” *Elements* **11**, 171–176 (2015).
- F. C. Hawthorne, R. Oberti, G. E. Harlow, W. V. Maresch, R. F. Martin, J. C. Schumacher, and M. D. Welch, “Nomenclature of the amphibole supergroup,” *Am. Mineral.* **97**, 2031–2048 (2012).

- T. Holland and J. Blundy, “Non-ideal interactions in calcic amphiboles and their bearing on amphibole-plagioclase thermometry,” *Contrib Mineral Petrol* **116** (4), 433–447 (1994).
- T. J. B. Holland, E. C. R. Green, and R. Powell, “Melting of peridotites through to granites: A simple thermodynamic model in the system KNCFMASHTOCr,” *J. Petrol.* **59** (5), 881–900 (2018).
<https://doi.org/10.1093/petrology/egy048>
- M. A. Kieffer, S. A. S. Dare, O. Namur, and E. T. Mansur, “Apatite chemistry as a petrogenetic indicator for mafic layered intrusions,” *J. Petrol.* **65** (4), 1–28 (2024).
- C. L. Kirkland, C. Yakymchuk, K. Szilas, N. Evans, J. Hollis, B. McDonald, and N. J. Gardiner, “Apatite: A U–Pb thermochronometer or geochronometer?,” *Lithos* **318–319**, 143–157 (2018).
<https://doi.org/10.1016/j.lithos.2018.08.007>
- L. N. Kogarko, “Chemical composition and petrogenetic implications of apatite in the Khibiny apatite-nepheline deposits (Kola Peninsula),” *Minerals* **8** (11), 532 (2018).
<https://doi.org/10.3390/min8110532>
- N. Kärkkäinen and H. Appelqvist, “Genesis of a low-grade apatite–ilmenite–magnetite deposit in the Kauhajärvi gabbro, western Finland,” *Miner. Deposita* **34**, 754–769 (1999).
- A. J. Locock, “An Excel spreadsheet to classify chemical analyses of amphiboles following the IMA 2012 recommendations,” *Comput. Geosci.* **62**, 1–11 (2014).
- G. Manhes, J. E. Minster, and C. J. Allegre, “Comparative uranium–thorium lead and rubidium–strontium study of the Severin Amphoterite: Consequences for early Solar System chronology,” *Earth Planet. Sci. Lett.* **39** (1), 14–21 (1978).
- A. E. Marfin, T. A. Radomska, A. V. Ivanov, V. S. Kamenetsky, M. B. Kamenetsky, T. Yu. Yakich, I. F. Gertner, S. L. Kamo, R. E. Ernst, N. V. Bryanskiy, O. M. Glazunov, and O. Yu. Belozero, “U–Pb dating of apatite, titanite and zircon of the Kingash mafic–ultramafic massif, Kan Terrane, Siberia: From Rodinia break-up to the Reunion with the Siberian Craton,” *J. Petrol.* **62** (9) (2021).
<https://doi.org/10.1093/petrology/egab049>
- J. Mikova and P. Denkova, “Modified chromatographic separation scheme for Sr and Nd isotope analysis in geological silicate samples,” *J. Geosci.* **52** (3), 221–226 (2007).
- G. O’Sullivan, D. Chew, G. Kenny, I. Henrichs, and D. Mulligan, “The trace element composition of apatite and its application to detrital provenance studies,” *Earth Sci. Rev.* **201**, 103044 (2020).
- P. M. Piccoli and P. A. Candela, “Apatite in igneous systems,” *Rev. Mineral. Geochem.* **48**, 255–292 (2002).
- N. Riel, B. J. P. Kaus, E. C. R. Green, and N. Berlie, “MAGEMin, an efficient Gibbs energy minimizer: Application to igneous systems,” *Geochem. Geophys. Geosyst.* **23** (7), 1–27 (2022).
- G. M. Saranchina, “Petrology of the Velimiyki intrusion and associated ore occurrence,” *Izv. Karelo-Finsk. Nauchn.-issled. Bazy AN SSSR* **2**, 32–42 (1948).
- Yu. A. Shukolyukov, I. M. Gorokhov, and O. A. Levchenkova, *Graphical Methods of Isotope Geology* (Nedra, Moscow, 1974).
- T. Tanaka, H. Kamioka, S. Togashi, and C. Dragusanu, “JNdi-1: A neodymium isotopic reference in consistency with LaJolla neodymium,” *Chem. Geol.* **168**, 279–281 (2000).
- P. Vermeesch, “IsoplotR: a free and open toolbox for geochronology,” *Geosci. Front.* **9** (5), 1479–1493 (2018).
- E. B. Watson, “Apatite saturation in basic to intermediate magmas,” *Geophys. Res. Lett.* **6** (12), 937–940 (1979).
- J. D. Webster and P. M. Piccoli, “Magmatic apatite: a powerful, yet deceptive, mineral,” *Elements* **11**, 177–182 (2015).
- D. L. Whitney and B. W. Evans, “Abbreviations for names of rock-forming minerals,” *Amer. Mineral.* **95**, 185–187 (2010).

Translated by M. Bogina

Publisher’s Note. Pleiades Publishing remains neutral with regard to jurisdictional claims in published maps and institutional affiliations. AI tools may have been used in the translation or editing of this article.